REPORT DOCUMENTATION PAGE

Form Approved
OMB No. 0704-0188

1. REPORT DATE *(DD-MM-YYYY)*	2. REPORT TYPE	3. DATES COVERED *(From - To)*
20-08-2009	Technical Paper	

4. TITLE AND SUBTITLE

Total and Differential Sputter Yields of Boron Nitride Measured by Quartz Crystal Microbalance (Preprint)

5a. CONTRACT NUMBER

5b. GRANT NUMBER

5c. PROGRAM ELEMENT NUMBER

6. AUTHOR(S)
B. Rubin, J.L. Topper, & A.P. Yalin (Colorado State University)

5d. PROJECT NUMBER

5e. TASK NUMBER

5f. WORK UNIT NUMBER
33SP0853

7. PERFORMING ORGANIZATION NAME(S) AND ADDRESS(ES)

Air Force Research Laboratory (AFMC)
AFRL/RZST
4 Draco Drive
Edwards AFB CA 93524-7160

8. PERFORMING ORGANIZATION REPORT NUMBER

AFRL-RZ-ED-TP-2009-319

9. SPONSORING / MONITORING AGENCY NAME(S) AND ADDRESS(ES)

Air Force Research Laboratory (AFMC)
AFRL/RZS
5 Pollux Drive
Edwards AFB CA 93524-7048

10. SPONSOR/MONITOR'S ACRONYM(S)

11. SPONSOR/MONITOR'S NUMBER(S)
AFRL-RZ-ED-TP-2009-319

12. DISTRIBUTION / AVAILABILITY STATEMENT

Approved for public release; distribution unlimited (PA #09383).

13. SUPPLEMENTARY NOTES
For 31st International Electric Propulsion Conference (IEPC 09) to be held in Ann Arbor, MI from 20-24 September 2009.

14. ABSTRACT

We present differential sputter yield measurements of boron nitride due to bombardment by xenon ions. A four-grid ion optics system is used to achieve a collimated ion beam at low energy (<100 eV). A quartz crystal microbalance (QCM) is used to measure differential sputter yield profiles of condensable components from which total sputter yields can also be determined. We report total and differential sputter yields of three grades of boron nitride due to bombardment by xenon ions for ion energies in the range of 60-500 eV and ion incidence angles of 0°, 15°, 30°, and 45° from normal. We also present preliminary results of the temperature dependence of the sputter yield. Comparisons with published values are made where possible

15. SUBJECT TERMS

16. SECURITY CLASSIFICATION OF:			17. LIMITATION OF ABSTRACT	18. NUMBER OF PAGES	19a. NAME OF RESPONSIBLE PERSON
a. REPORT	b. ABSTRACT	c. THIS PAGE			Justin Koo
Unclassified	**Unclassified**	**Unclassified**	SAR	19	19b. TELEPHONE NUMBER *(include area code)* N/A

Total and Differential Sputter Yields of Boron Nitride Measured by Quartz Crystal Microbalance (Preprint)

IEPC-2009-042

Presented at the 31st International Electric Propulsion Conference,
University of Michigan • Ann Arbor, Michigan • USA
September 20 – 24, 2009

B Rubin[1], J. L. Topper[2] and A. P. Yalin[3]
Colorado State University, Fort Collins, Colorado 80523, USA

We present differential sputter yield measurements of boron nitride due to bombardment by xenon ions. A four-grid ion optics system is used to achieve a collimated ion beam at low energy (<100 eV). A quartz crystal microbalance (QCM) is used to measure differential sputter yield profiles of condensable components from which total sputter yields can also be determined. We report total and differential sputter yields of three grades of boron nitride due to bombardment by xenon ions for ion energies in the range of 60-500 eV and ion incidence angles of 0°, 15°, 30°, and 45° from normal. We also present preliminary results of the temperature dependence of the sputter yield. Comparisons with published values are made where possible.

Nomenclature

A_s	=	QCM sensor area
E	=	ion energy
E^*	=	characteristic energy describing the differential sputter yield profile shape
E_{th}	=	threshold sputtering energy
$J_{B,avg}$	=	time-averaged current of ions and energetic neutrals incident on the target
k	=	fitting coefficient
M_B	=	boron atomic mass
M_N	=	nitrogen atomic mass
R	=	mass accumulation rate
r_{qcm}	=	distance from the target center to the QCM
Y_{BN}	=	full BN sputter yield
Y, Y_{QCM}	=	deposited condensable sputter yield
y, y_{MZ}	=	volumetric differential sputter yield
α	=	ejection polar angle of sputtered atoms measured relative to the surface normal
β	=	incidence angle of bombarding ions measured relative to the surface normal
ϕ	=	ejection azimuthal angle of the sputtered atoms measured in the plane of the target surface
ρ	=	density of the target material

I. Introduction

ION sputtering is a primary life-limiting mechanism in electric propulsion (EP) thrusters used for satellite and space exploration[1-12]. Owing to the relatively long lifetimes (5-10+ years) of EP thruster devices and the complexity and expense of experimental tests, effects of sputter erosion and deposition are often studied with

[1] Postdoctoral researcher, Department of Mechanical Engineering, brubin@engr.colostate.edu
[2] Graduate student, Department of Mechanical Engineering, jim.topper@rams.colostate.edu
[3] Associate professor, Department of Mechanical Engineering, ayalin@engr.colostate.edu

numeric codes. For erosion (lifetime) studies, the aim is to compute the amount of surface erosion due to the bombarding ions. Such modeling requires knowledge of the total sputter yields (Y) of the eroding materials at the ion conditions (energy and incidence angle) of interest. Deposition modeling additionally requires differential (angular) sputter yields ($y(\alpha,\phi)$) in order to track the trajectories of sputtered particles. Total and differential sputter yield profiles have been measured with a multitude of techniques, a partial list of which includes weight loss[10,12], collector plates[13-14], mass spectrometry[15], quartz crystal microbalance[3-7,9-11,16-17], Rutherford backscattering[18-19], radioactive tracers [20], and cavity ring-down spectroscopy [21-22].

We are specifically interested in the sputtering of boron nitride (BN) because of its widespread use as an insulator material in the acceleration channel of stationary plasma thrusters (SPTs). Erosion of the insulator channel is the dominant thruster life-limiting mechanism in SPTs. Sputter erosion removes material from the channel wall and eventually exposes the underlying magnetic yoke, causing the magnetic field profile to be altered and the end of life to be reached. Furthermore, deposition of the sputtered BN can contaminate spacecraft surfaces (e.g. solar panels or thermal control surfaces). Despite the importance of BN erosion there is a lack of basic sputtering data on BN. Numerical modeling of thruster erosion[23-25] shows that the ions most critical to the erosion process have relatively low energy (≤100 eV). Measurements in this energy range are challenging since the low sputter yields can lead to signals below the detection sensitivity of the measurement system; additionally, it can be difficult to obtain collimated monoenergetic ion beams at these energies. The goal of the present study is to contribute towards filling this gap. In this work we detail development of an experimental configuration for low energy BN sputter measurements. We report differential and total sputter yields for several grades of BN at ion energies down to 60 eV, obtained with a QCM deposition sensor[3-7,9-11,16-17]. In section II we discuss the experimental apparatus and procedures used for data analysis. Results of validation measurements performed by using molybdenum as a control are presented in section III. Section IV contains a summary of the experimental results, including total and differential sputter yields of HBC, HBR, and HP grades of boron nitride under bombardment by xenon ions. Comparisons with available published values are provided. Finally, conclusions are given in section V.

II. Experimental Apparatus and Procedure

A. Overview of Sputter Measurement System

Total and differential sputter yields are measured using a quartz crystal microbalance (QCM) deposition monitor. The experimental apparatus is shown in Fig. 1. The main elements of the system have been previously described[5-7, 9-11,26]. In this subsection we give an overview of its essential features, while the following subsections detail specific aspects and recent modifications. An improvement relative to our past work[7] is that both weight loss and QCM

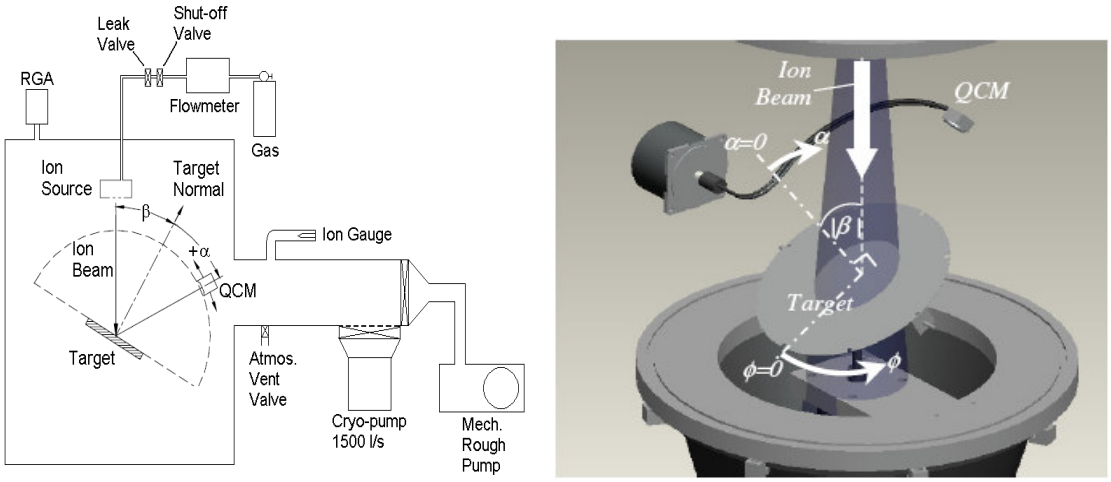

Figure 1. Left: Schematic diagram of experimental set-up. Right: Solid-model showing angle definitions.

measurements are performed concurrently in the same facility. The role of weight loss measurements is discussed below. The ion source and QCM are housed within a 0.125 m^3 stainless steel vacuum chamber (43 cm ID x 76 cm long main section), equipped with a 1500 liter/s cryogenic pump (CTI-8). The chamber base pressure is 5×10^{-5} Pa giving a working pressure of approximately 2 to 5×10^{-3} Pa (corrected for Xe). Based on the chamber pressure and

temperature, the mean free path for boron atoms (i.e. sputtered particles) is 1.7 m such that ~10% of the boron atoms will experience a collision with background xenon atoms before reaching QCM surface (17.4 cm away). Some particles will therefore be deflected prior to reaching the QCM (lowering the measured yield), but other particles not originally directed at the QCM will be deflected to deposit on it. The effect of these collisions is hard to estimate exactly but is at most 10% which, as compared to the 30% uncertainty on reported yields, is considered to be negligible. The DC ion source with two-grid and four-grid ion optics, specially designed for low energy operation, is described below in more detail. A rotatable target-mount is positioned 23 cm downstream of the ion source. As shown in Fig. 1, the QCM is rotated in an arc above the target and the target itself is rotated azimuthally. Combinations of these movements allow us to probe over the hemisphere above the target, thereby obtaining differential sputter yield profiles. Both the QCM and target rotation are performed using 25000 step stepper motors, which are controlled using a motion control system (Parker CompuMotor). A personal computer with LabView is used for data logging. Detailed discussion of the QCM sensor is provided in subsection IIF.

B. Definition of Angles

The angles used to describe the direction of ion incidence and the ejections angles of sputtered particles are shown in Fig. 1. We define as follows: β is the incidence angle of bombarding ions measured relative to the surface normal (β=0 for normal incidence), α is the ejection polar angle of sputtered atoms measured relative to the surface normal, and ϕ is the ejection azimuthal angle of the sputtered atoms measured in the plane of the target surface (defined so that ϕ=0 is in the forward sputter direction i.e. in the forward direction of the plane containing the surface normal and the incident ion directions).

C. Ion Source

A DC Kaufman ion source using a dual thoriated tungsten filament as a discharge cathode and thoriated tungsten filament as a neutralizer is used[11]. The four-grid ion optics system, designed using an in-house ffx code[26, 27] and fabricated in-house, produces collimated beams at the low ion energies of interest to this work (20-350 eV). For higher energy measurements (250 – 500 eV), a two-grid ion optics system is used. Both grid sets can be used for the 250-350 eV range and the results obtained using two grid sets are similar. For both grid sets, typical beam parameters include a xenon flow rate of 0.05 mg/s, a beam current of 1-4 mA, a discharge voltage of 20 to 40 V, and a (beam) neutralizer current of 150% of the beam current. During measurements, the ion current leaving the source is recorded. Determination of the sputter yield requires knowledge of the current of energetic particles (ions and fast neutrals) incident on the sputtering target. As in our past work[9-11], we make corrections for charge-exchange and scattering. The charge-exchange beam generates fast neutrals which, depending on scattering angles, may bombard the target. The resulting correction is to multiply the measured source current by 0.8-0.95, depending on the chamber pressure and ion energy.

Ion source characterization was performed to determine the bombardment conditions[26]. The beam divergence angle, defined as the angle from normal including 90% of the beam current, was found as 12° from a beam profile measured with a collimated Faraday probe (the divergence angle increases slightly with beam energy), corresponding to a beam diameter of approximately 13.5 cm at the sample plane. A four-grid retarding potential analyzer (RPA) was used to measure the ion energy distribution, yielding a full width at half maximum (FWHM) of 6-19 V, increasing with beam energy. To determine the charge states of the ions an ExB probe was used. No triply charged ions were detected. The average double-to-single number density ratio was $\leq$5% for beam energies between 80 eV and 250 eV, dropping with decreasing energy. For beam energies below 80 eV the number density of doubles fell below the detection limit (1%). The doubly-charged ions have twice the energy of singles but are counted as two charges in the current measurements. Because the measured yields are relatively linear and the fraction of doubles is low, simple estimates show their effect to be negligible.

D. Boron Nitride Targets, Surface Charging, and Moisture Effects

Test results reported herein are for HBC, HBR, and HP grades of Boron Nitride (BN). Each of these materials is formed by hot-pressing and corresponds to the graphite-like allotrope of BN. In the base plane, atoms are held together by strongly directed hexagonal arrays of covalent bonds, resulting in unique electrical, thermal, and mechanical properties. The HBC and HBR materials were obtained from General Electric's Advanced Ceramics (currently Momentive Performance Materials). Calcium borate is used as binder in HBR, while no binder is used in HBC. The two grades have generally similar properties though with some differences. For example, HBR has higher thermal expansion, higher moisture absorption, and higher volume resistivity at elevated temperatures. The HP grade is obtained from Saint-Gobain and uses calcium borate as binder. Figure 2 shows Scanning Electron

Microscope (SEM) pictures of HBC grade BN in an unsputtered state and after 15 hours of sputtering by a 250 eV Xe ion beam (ion dose – 3x1019 ions/cm2). Little change can be detected in the surface structure.

Our past measurements of insulator materials, including boron nitride, have shown effects of surface charging and the importance of appropriate neutralization[9-11]. Similar surface charging effects have been observed by Zhang et al.[28] and Nikiporetz et al.[29]. In order to neutralize the surface charge, a plasma bridge neutralizer (PBN) is placed in the chamber close to the target. Details on the neutralization scheme are discussed in our past work[9-11] and Section IVA below. The operating conditions of the PBN are an emission current of 10-15 mA and a Xe mass flow rate of 0.5 sccm. The PBN was biased at negative 15 V relative to ground potential.

During QCM measurements, the total sputter yields were also measured using a weight loss technique, but the results displayed poor reproducibility and are not reported here. The limitations of the weight loss measurements are largely owing to moisture absorption by the samples during times when the samples are exposed to atmosphere (in

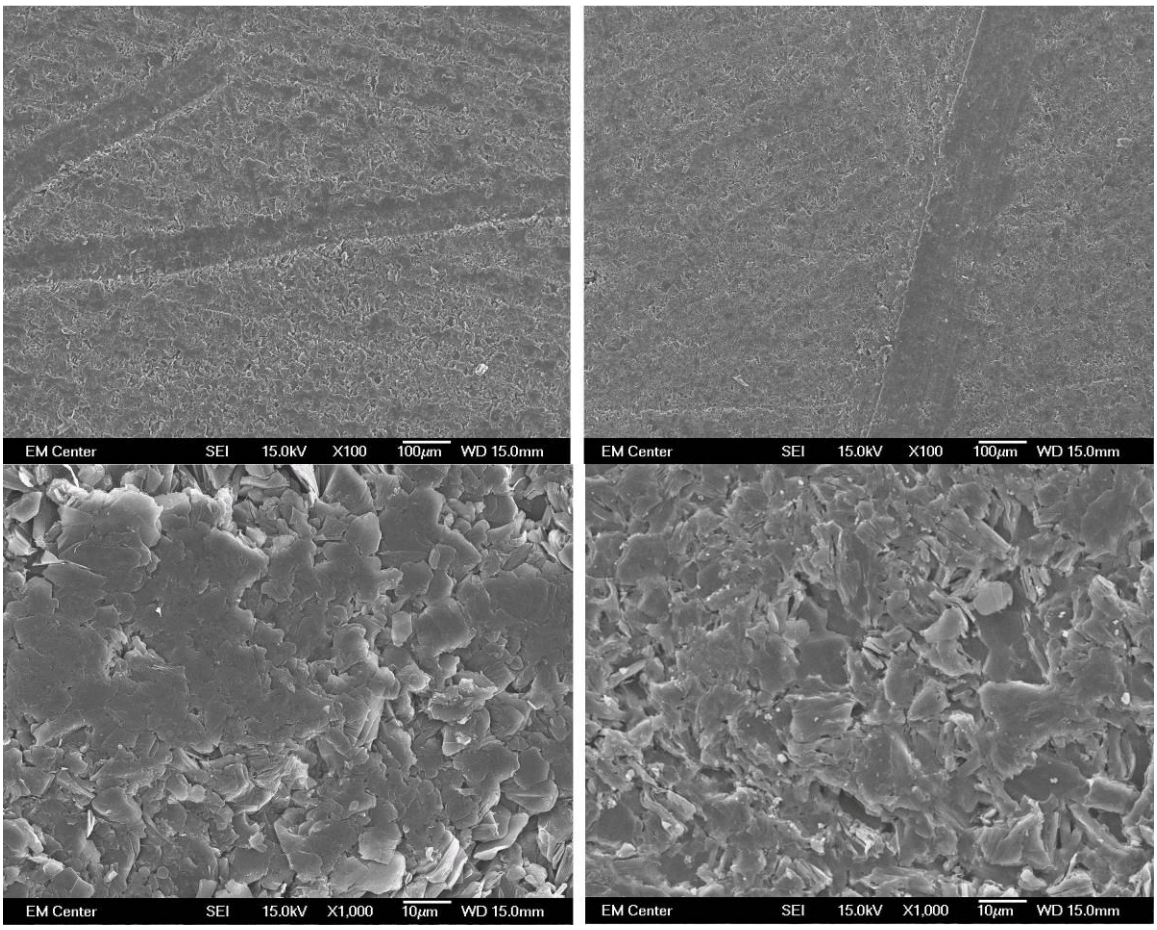

Figure 2. Scanning Electron Microscope images of HBC BN surface. Left: Unsputtered surface. Right: Sputtered with 250 eV Xe+ ions for 15 hours.

principle, the weightings could be done within the vacuum chamber, but this is impractical in our setup). Moisture absorption and associated mass change were observed for all grades of BN[10,11] and are expected based on material datasheets and similar observations by Garnier[30]. HBC has the lowest moisture pickup, followed by HBR and HP. The latter two can maintain appreciable amounts of moisture even after storage in a dry environment (likely due to the binder). For HBR the mass buildup levels off after approximately one hour of atmospheric exposure, while as shown in Fig. 3 the mass buildup of HP is at a higher rate and for a longer duration. For all grades, the large mass buildup (and variation of individual samples) relative to the total mass change of a typical sputter test (~2-10 mg) precludes accurate sputter yield determination from mass loss measurements in our current setup. The relative humidity in the laboratory was in the range of 20-40% during these measurements. Of course, such effects do not influence QCM measurements.

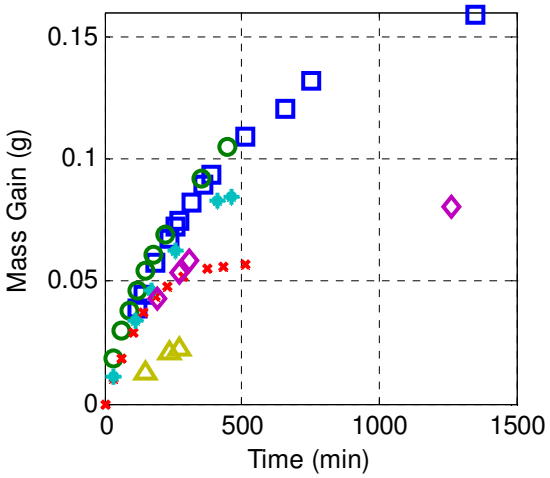

Figure 3. Mass change as a function of time of atmospheric exposure for six different HP BN samples. Zero time corresponds to 90 minutes after removal from vacuum chamber, and mass gain is relative to sample mass at 90 minutes. The starting total sample mass is approximately 150 g.

Another phenomenon that can influence weight loss measurements is xenon ion implantation into the sample. If a significant number of xenon ions are implanted in the sample, the measured mass loss and apparent sputter yield would be reduced. To check the influence of ion implantation, X-ray photoelectron spectrometry (XPS) analysis was performed on a HBC BN sample using a PHI 5800 XPS system. A previously unused sample was sputtered for 15 hours with a 250 eV ion beam (ion dose – 3x1019 ions/cm2) after which XPS analysis was performed. The analysis shows implanted xenon with an atomic fraction of 0.1%. Angularly resolved XPS measurements show that the implanted xenon is only in a thin near-surface layer. The measured atomic fraction versus electron emission angle is shown in Fig. 4. The increase of atomic fraction with angle shows that the depth of xenon implantation does not exceed a few nanometers. From the point of view of weight loss, simple numeric estimates show that the mass of implanted xenon is negligible compared to the mass change due to sputtering.

E. Boron Nitride Sputter Products

In deposition mode, the QCM allows determination of differential sputter yields through measurement of mass accumulation (of sputtered particles) on its surface. For condensable components, sticking coefficients are assumed to be unity. Note that sticking coefficients for "new layers" and very thin layers (typically 10's of Angstroms) may be less than unity, but once a sufficient layer thickness of a given material has accumulated, sticking coefficients for condensables are generally unity [31]. As will be further discussed, the sputtered particles from BN may consist of a mix of condensable and non-condensable components.

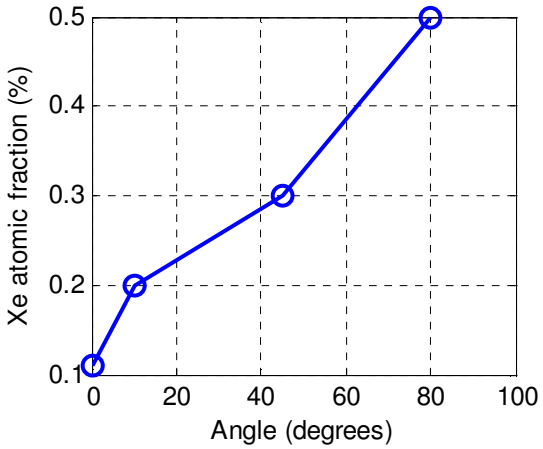

Figure 4 . Angularly resolved XPS measurements of Xe in BN target.

To study the chemical composition of the layer deposited on the QCM surface during the BN sputter yield measurements, the surface of the QCM as well as a HBC BN target were analyzed using XPS. For the QCM surface layer, B 1s and N 1s spectral lines were detected in a proportion of 5.5:1 B:N. It is important to realize that these features are due to all of the corresponding material regardless of atomic or molecular composition, e.g. the B 1s is due to boron from boron atoms, BN, oxides etc. Therefore, the 5.5:1 ratio immediately indicates that sputtering is predominantly as atoms of B and N (or possibly Bx and Ny) but not so much as BN or other BxNy, since there is much more B on the QCM relative to N). We make this conclusion under the assumption the B atoms (or Bx) condense onto the QCM while N or N2 does not. We use the NIST XPS database[32] for line assignments and other features of the spectra are as follows. There is variation in reported B 1s line locations, but the consensus is that pure atomic B is at 186-188 eV, B from BN is at ~190-191 eV, and B from B2O3 is at ~192-194 eV. Atomic B is not detected in the target or QCM surface likely because it oxidizes (to B2O3) in the atmosphere (and the materials were exposed to atmosphere prior to the XPS measurements). Clearly the BN feature is large from the BN target (which shows both BN and B2O3) but small from the QCM surface (consistent with our hypothesis). In summary, the salient point is that the majority of the

B detected in the QCM surface is in the form of B2O3 as would be expected if sputtering of B is predominantly is predominantly as B atoms, or Bx, (but not as BN) which deposit on the QCM and subsequently oxidize.

Sputtering predominantly as atoms is also consistent with past mass spectrometry results[1,33] and multi-

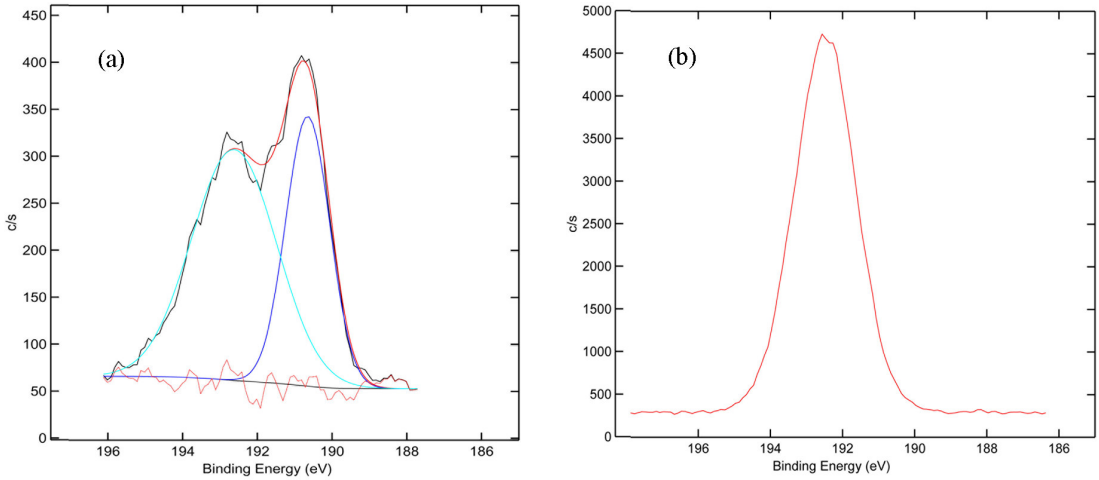

Figure 5. XPS results for the HBC BN target (a) and QCM surface (b). For the HBC BN target, fitted peaks (and their sum) are shown.

component sputtering theory. The XPS analysis of a sputtered BN sample performed by Garnier[30] demonstrated little variation between the boron and nitrogen fractions in the sample before and after sputtering, which suggests that boron and nitrogen are sputtered at approximately equal rates as would be expected based on the bulk composition. Therefore, assuming sputtering as atoms with only B depositing on the QCM, the full BN yield is related to the deposited condensable yield as

$$Y_{BN} = Y_{QCM} \cdot \frac{M_B + M_N}{M_B} \tag{1}$$

where MB is the mass of boron, MN is the mass of nitrogen, YQCM is the QCM-measured yield, and YBN is the full BN yield (this equation applies for both differential and total yields). Owing to the reactivity of atomic nitrogen, it is also possible that N atoms form N2 as they leave the surface, but in the case of sputter products being B and N2 (with B depositing on the QCM), equation (1) still holds.

F. QCM Sensor and Measurement Procedure

We use a deposition controller (Sigma Instruments SQC-339) that reads the crystal frequency to 0.001 Hz and an RC-cut quartz crystal as opposed to the more conventional AC-cut crystal. The RC-cut crystal (Tangidyne Corporation) is very accurate for deposition of thin films. Increased sensitivity is achieved by adjusting the stress coefficients of the quartz plate using advanced fabrication methods

The quartz crystal resonance frequency is extremely sensitive to temperature variation so the QCM should be maintained at constant temperature during measurements. A programmable digital temperature controller with refrigerating/heating circulator (PolyScience 9002) is used to control the temperature of the QCM. The water circulates through the stainless steel body of the QCM housing with the temperature of the water bath controlled to $\pm 0.01^{o}$C. As the crystal is moved to different positions its incident the heat flux varies; therefore, although the temperature of the water stays constant, the actual crystal temperature is different at different locations (α angles). A K-type thermocouple wire embedded in a copper holder silver-soldered to the back of the QCM crystal holder monitors QCM temperature, and each sputter yield measurement is started only after the temperature of the crystal has stabilized.

For a given incidence angle β (obtained by tilting the target), the differential sputter yield profile is obtained by measuring the sputter yield over two chords above the target: ϕ=0°/180° and ϕ = 60°/240° (where the latter, by symmetry, also corresponds to ϕ=120°/300° for azimuthally symmetric sputtering profiles). A total of 34-36

positions above the target are typically sampled. At a given measurement point the volumetric differential sputter yield, $y(\alpha,\phi)$, in units of mm^3/C/sr, is determined using

$$y(\alpha,\phi) = \frac{\left[R(\alpha,\phi) r_{qcm}{}^2 \right]}{\left[\rho J_{B,avg} A_s \right]} \tag{2}$$

where $R(\alpha, \phi)$ is the measured mass accumulation rate (found from the QCM's deposition monitor device), ρ is the density of the target material (close to 2 mg/cm^3 for all grades of BN used), $J_{B,avg}$ (C/s) is the time-averaged current of bombarding particles (ions and energetic neutrals) incident on the target, r_{qcm} is the distance from the target center to the QCM (17.4 cm), and A_s is the QCM sensor area (0.535 cm^2). The quantity $A_s/r_{qcm}{}^2$ corresponds to the solid angle that the QCM sensor subtends while $R(\alpha, \phi)/\rho J_{B,avg}$ corresponds to the volume of sputtered material per bombarding charge. It is important to emphasize that the directly measured quantity is the mass buildup of condensable particles on the QCM and the volumetric differential sputter yield should be considered in this way. (In fact the "volume" may not really correspond to any physically observed volume since it corresponds to the equivalent volume due to the mass of the *deposited material* if one uses the density of the full *target material*; of course conversion to the deposited mass yield simply requires removing the density from (2)). Finally, as discussed in subsection IIE, equation (1) can be used to convert the measured QCM yield (from (2)) to the corresponding full BN yield.

G. QCM Signal Analysis.

Analysis and fitting of differential sputter yield profiles requires appropriate functional forms. At our conditions, stopping is predominantly due to elastic (nuclear) collisions and is generally in the linear cascade regime (emitted particles are secondary or higher generation recoils) or single knock-on regime (emitted particles are primary recoils)[1]. A classical theory for the linear cascade regime was originally developed by Sigmund[35]. Independent of ion incidence angle, the original Sigmund theory predicts sputtering profiles that are azimuthally symmetric and approximately diffuse in shape, corresponding to cosine-like profiles of the form $y \sim \cos(\alpha)^n$ (n=1 for a diffuse profile). More recent experimental and numerical studies show a range of profile shapes. For normally incident ions on polycrystalline and amorphous targets, cosine-like profiles are generally observed with increasingly under-cosine shapes as ion energy is lowered and increasingly over-cosine shapes for higher ion energies[5-7,9-10,15,35-37]. For obliquely incident ions at relatively high ion energy, observed profiles also tend to be azimuthally symmetric. However, for lower ion energies the measured profiles tend to be asymmetric with increased sputtering in the forward direction[5-7,9-10,16,20,35]. Similar profiles have been modeled on a theoretical basis[37-39].

As a means to describe the measured differential sputter yield profiles we use expressions from Zhang[40], based on work from Yamamura[38-39], to which we introduce two fit parameters. We term the resulting expressions as Modified Zhang (MZ)[7]:

$$y_{MZ} = \frac{Y}{1-\sqrt{\frac{E^*}{E}}\cos(\beta)} \cdot \frac{\cos(\alpha)}{\pi} \left[1 - \frac{1}{4}\sqrt{\frac{E^*}{E}} \left(\cos(\beta)\gamma(\alpha) + \frac{3}{2}\pi \sin(\beta)\sin(\alpha)\cos(\phi) \right) \right] \tag{3a}$$

$$\gamma(\alpha) = \frac{3\sin(\alpha)^2 - 1}{\sin(\alpha)^2} + \frac{\cos(\alpha)^2 \left(3\sin(\alpha)^2 + 1 \right)}{2\sin(\alpha)^3} \ln\left(\frac{1+\sin(\alpha)}{1-\sin(\alpha)} \right) \tag{3b}$$

where y_{MZ} is the differential sputter yield, Y is the total sputter yield, E is the ion energy, E^* is a characteristic energy describing the profile shape, and the angles are as defined above (the expression is properly normalized so that integrating the differential sputter yield, y_{MZ}, over the sputtering hemisphere gives Y). The formulation decouples the amplitude and shape of the profiles through the use of Y and E^* respectively. More recent work by Zhang et al.[40] also discusses the use of a varying energy parameter. In general, rather than using the MZ expressions for *a priori* calculation, we treat Y and E^* as free fit-parameters which we determine from (least-squares fitting)

experimental data. Note that profile shapes are determined by the ratio E^*/E and for high ion energy ($E^*/E << 1$) the MZ expression reduces to the diffuse yield ($y=Y\cos(\alpha)/\pi$).

H. Measurement Procedure

Targets are pre-sputtered to better represent the conditions found in long-duration EP operating applications. Pre-sputtering of HBC and HBR samples is by a 500 eV ion beam with a current density of ~0.1 mA/cm² for 15 hours, while the HP sample is pre-sputtered by a 750 eV ion beam with a current density of ~1 mA/cm² for 2 hours. An order-of-magnitude estimate for the typical dose of incident ions on a target prior to testing is 1019 ions/cm2 (corresponding to a sputtered surface thickness of several microns). Target contamination effects are estimated to be negligible, since for typical conditions the flux of ions incident on the target is approximately 10 times higher than the flux of nitrogen (the major contaminant) to the target[7]. The samples are also heated under the chamber filaments for at least 30 minutes prior to sputtering to remove moisture and to reach thermal steady-state. Test durations are fixed such that the QCM has time (at each position) to sufficiently stabilize relative to thermal and background noise. Test times vary from several hours for higher energy tests to as long as 20 hours for lower energy tests, corresponding to the ion doses of 6.7x1018-4.5x1019 ions/cm2.

III. Measurement System Validation

Validation of our sputter yield measurements is performed by using molybdenum as a control. While there is variation in data from different research groups, molybdenum sputter yields are reasonably well characterized[3,6,7,42,43]. We have measured the total sputter yield of Mo at normal incidence at energies of 150, 250 and 350 eV. As shown in Fig. 6, the total yields (found from the Y parameter of the best-fit MZ profile) are self-consistent and in reasonable agreement with the Yamamura and Tawara curve fit[42-43]. The currently reported yields (shown as CSU 2008) are somewhat lower than those previously measured using the same apparatus with two-grid ion optics (shown as CSU 2007) though the difference is within experimental uncertainty[7]. Although our values are approximately a factor of two lower then Kolasinski's (measured by etching a thin Mo layer off the QCM surface)[3], they are in good agreement with the data of Doerner[44] (weight loss method). These results are taken as validation of the measurement methods and in particular of the assumption that the sticking coefficient of the QCM may be taken as unity for condensables.

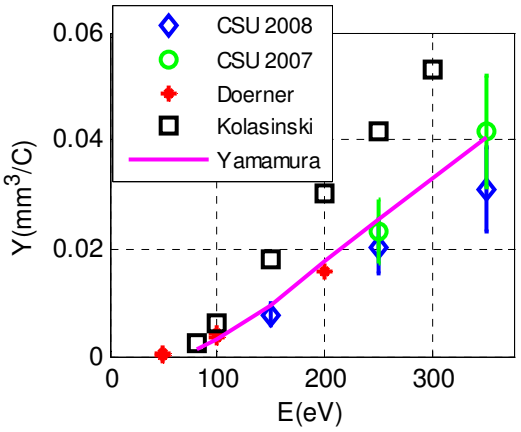

Figure 6. Total sputter yield versus ion energy for normal incidence, Xe^+ on Mo.

IV. Results & Discussion

A. Total Sputter Yields

Figure 7 shows total sputter yields of the three BN grades, determined from the Y parameter of the best-fit MZ profile (equivalent to integrating the best-fit differential profile) as a function of ion energy for normal incidence. The total yields of Fig. 7 (and Fig. 8) are only due to condensable particles depositing on the QCM, and equation (1) can be used to find the corresponding full BN yields. The measurements of total sputter yield values are performed multiple times for the majority of the data points. Measurements in the energy range of 60-350 eV are performed using the four-grid ion optics, while the range of 250-500 eV uses the two-grid ion optics. For the cases when several measurements were done at the same conditions, the average value is reported. Total sputter yields of HBC and HBR grades are nearly identical, although HP yields at 200 and 250 eV are somewhat higher. However, the differences between the yields of HP and the other two grades are likely not statistically significant as the differences are within the experimental uncertainty. Experimental uncertainty on measured differential sputter yields and total sputter yields are estimated to be about 30% based on the repeatability of the sputter yield measurements.

Where possible, we compare our total sputter yields with measurements and modeled values from other research groups. Figure 9 shows our recent measurements for HBC BN along with weight loss measurements by Semenov[46], Garnier[30], Abashkin[47], Kim[48], and modeled values from Yim[23]. In this case we have scaled our yields using (1) to

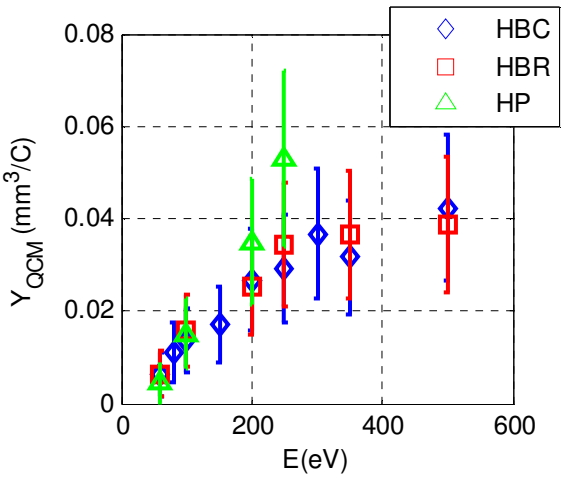

Figure 7. Total condensable sputter yield from QCM versus ion energy for normal incidence.

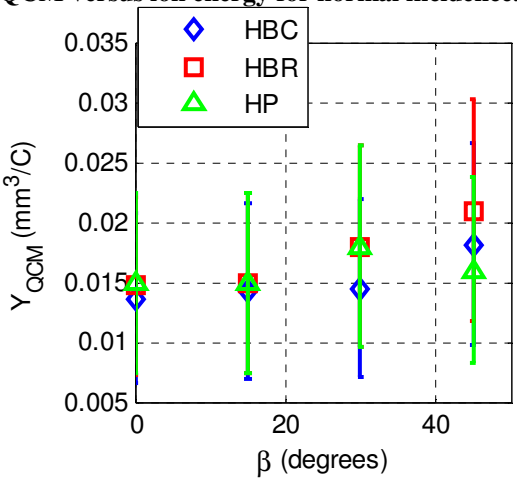

Figure 8. Total condensable sputter yield from QCM versus incidence angle for 100 eV ion energy.

represent full BN sputtering yields (not just the measured condensable particles). Not all of the authors specify the grade of BN used. The values we are currently reporting are high relative to past measurements. The difference in the measured sputter yields may be attributed to the difference in the properties of different BN grades (e.g. presence of binders). Even for a given BN grade produced by the same manufacturer, the material properties can vary. Comparison against weight loss measurements may be influenced by moisture effects as discussed in connection with Fig.3. Also, if samples have been heated, it is possible that surface changes have been induced. In terms of Yim's modeled values, certain details of the molecular binding were selected to achieve agreement with the published experimental data. Finally, inadequate surface neutralization may lead to low apparent yields as further discussed below. The validation measurements presented above suggest that if a systematic error is present in our data, it results in sputter yields that are lower, not higher, than true values.

The values reported here are also higher then the values we have previously reported using the weight loss method in a different vacuum chamber[10] likely owing to inadequate surface charge neutralization or variations in current density values in the previous work. While the latter would not lead to substantial error (<~30%), the former could be significant. A key differences in the present setup compared to that used for the past total yield measurements[10] is that the present setup allows real-time sputter measurements using the QCM. This capability allows us to select the emitted current from the PBN by monitoring its effect on the measured sputter yield. Initially the sputter rate increases with the neutralization current prior to reaching saturation when the target is adequately neutralized. Measurements reported here are safely in the saturated regime. In contrast, in the past setup the neutralization current was pre-selected based on the total beam current value and the neutralizer characteristics, and may have been inadequate for complete surface neutralization thereby leading to lower measured sputter yields.

B. Differential Sputter Yields

As described in subsection IIG, MZ expressions are used to fit the profiles and the parameter E*/E describes the shape of the profile. Figure 10 shows the variation in E*/E for normal incidence as a function of ion energy for the three grades of BN. In this energy range the parameter E*/E tends to increase with energy for all grades of BN but other apparent features (e.g. maxima) are likely not statistically significant (i.e. fall within the noise of the data). Figure 11 shows the variation in E*/E at 100 eV as a function of incidence angle for the three grades of BN. For HBC and HP grades the value of the parameter is almost

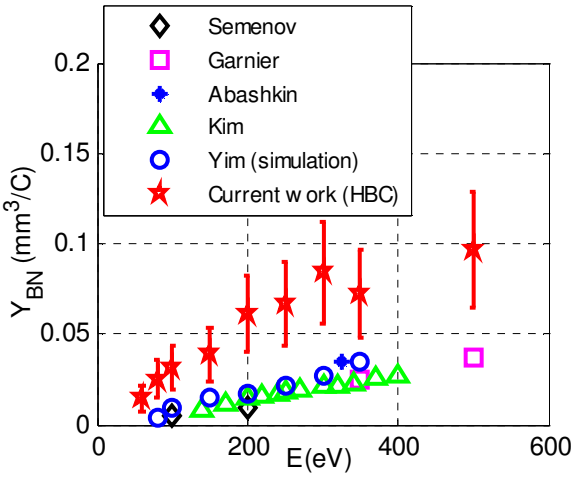

Figure 9. Total BN sputter yields as compared with published values.

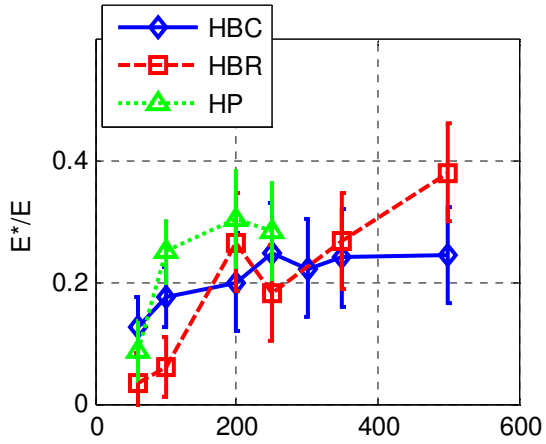

Figure 10. *E*/E* versus ion energy for normal incidence. (Points are joined with straight lines to guide the reader).

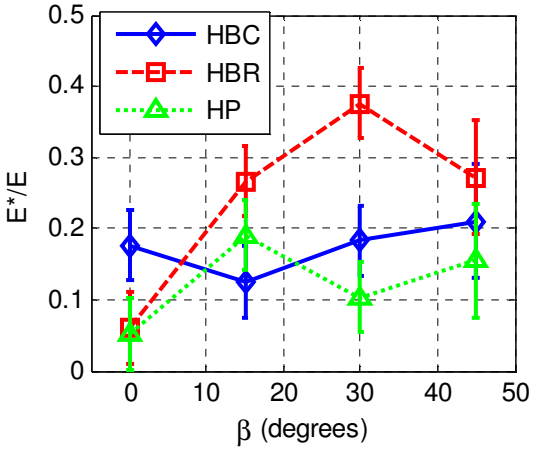

Figure 11. *E*/E* versus incidence angle for 100 eV ion energy. (Points are joined with straight lines to guide the reader).

independent of the incidence angle, for HBR it increases with the incidence angle. For all conditions studied, the values of E*/E indicate that the differential sputter yield profiles are non-diffuse. Error bars are estimated from the repeatability of the differential sputter yield measurements.

Examples of comparison between measured (raw) QCM data and fitted MZ profiles are given in Fig. 12 . Both plots are for xenon ion energies of 250 eV on HBC BN. The left plot is for normal incidence and the right plot for 30° incidence. The plots include QCM measured points, best-fit MZ profiles, and (for comparison) diffuse profiles with the same total yield. One can see agreement between the measured and MZ profiles. The fitted normally incident profile is azimuthally symmetric. The profile for 30° incidence corresponds to the forward/backward plane (φ=0/180°) and shows a forward sputter lobe (α<0) with reduced sputtering in the backward direction (α>0). In general, the MZ expressions provide reasonable descriptions of the measured profiles. The asymmetry of the non-normal incidence profiles and the disagreement with diffuse profiles in all cases illustrate the inadequacy of simply assuming diffuse profile shapes as has been done in some past research.

In Fig. 13-14, examples of the best-fit MZ differential sputter yields are shown using colored hemispheres. Colors (indicated in legend) correspond to the yield in the given direction. As discussed above, for normal incidence the profile is azimuthally symmetric, while for increasingly non-normal incidence the profiles show increasing forward sputter lobes. For 15° incidence the profile is already significantly azimuthally asymmetric.

In Tables 1-3 the best-fit MZ values are presented for all conditions and grades studied. The trends are generally similar to the ones presented above. Two total yield values are given for each condition: the directly measured QCM yield Y_{QCM}, and the scaled value from (1), representing full BN sputtering, Y_{BN}. Error bas are as discussed above.

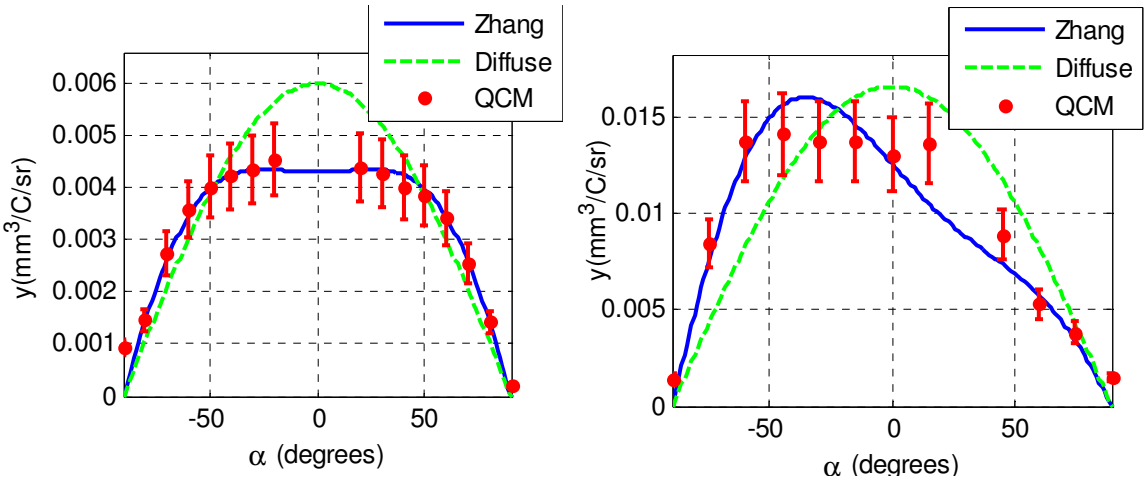

(a) (b)

Figure 12. Example of QCM data with best-fit MZ profiles for 250 eV ions on HBC at normal incidence (a), and at 30° (b).

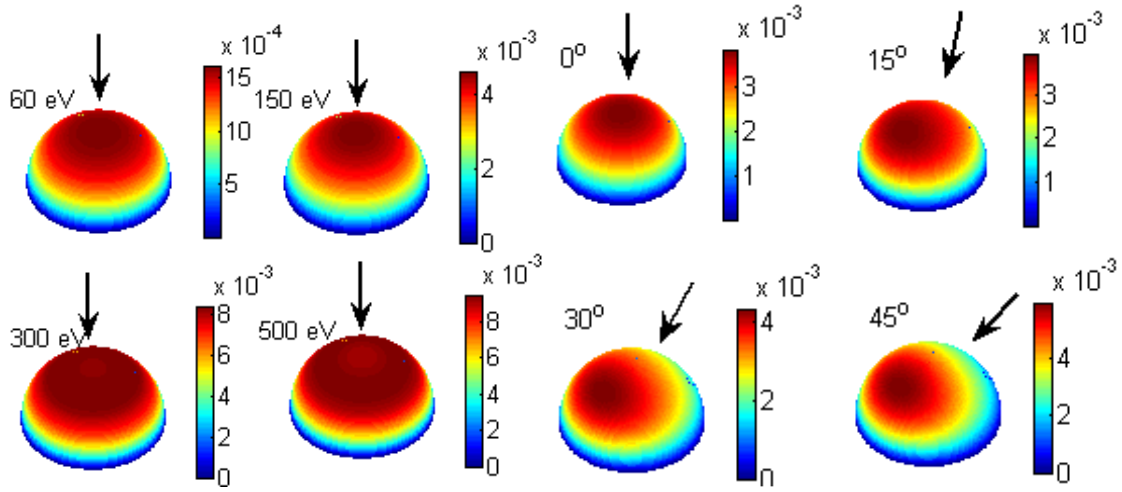

(a) (b)

Figure 13. Differential sputter yield profiles for HBC grade BN. Normal incidence and different beam energies (a). Varying incidence angles at a beam energy of 100 eV (b). Arrows show the direction of ion incidence. Units are mm^3/C/sr.

Table 1. Total Sputter Yields (Y) and Characteristic Energies (E^*) of HBC BN.

Ion energy (eV)	Incidence angle (°)	Y_{QCM} (mm^3/C)	Y_{BN} (mm^3/C)	E^* (eV)
60	0	0.0063	0.0145	8
100	0	0.0136	0.0312	18
100	15	0.0142	0.0327	13
100	30	0.0145	0.0333	18
100	45	0.0181	0.0417	21
150	0	0.0170	0.0390	13
200	0	0.0268	0.0614	40
250	0	0.0291	0.0669	63
250	15	0.0234	0.0539	65

250	30	0.0287	0.0660	96
250	45	0.0258	0.0594	86
300	0	0.0367	0.0842	67
350	0	0.0316	0.0726	84
350	15	0.0200	0.0459	97
350	30	0.0243	0.0559	148
350	45	0.0308	0.0707	163
500	0	0.0423	0.0973	123
500	15	0.0473	0.109	150
500	30	0.0485	0.112	207
500	45	0.0545	0.125	231

Table 2. Total Sputter Yields (Y) and Characteristic Energies (E^*) of HBR BN.

Ion energy (eV)	Incidence angle (^{o})	Y_{Cond} (mm^3/C)	Y_{BN} (mm^3/C)	E^* (eV)
60	0	0.0064	0.015	2
100	0	0.0158	0.036	6
100	15	0.0185	0.0425	27
100	30	0.0218	0.0502	38
100	45	0.0233	0.0535	27
200	0	0.025	0.058	53
250	0	0.034	0.079	46
250	15	0.0276	0.0634	58
250	30	0.0566	0.130	69
250	45	0.0497	0.114	97
350	0	0.0365	0.0838	94
350	15	0.0328	0.0753	134
350	30	0.0514	0.118	135
350	45	0.0644	0.148	182
500	0	0.0388	0.089	191
500	15	0.0669	0.154	213
500	30	0.0657	0.151	250
500	45	0.101	0.233	261

Table 3. Total Sputter Yields (Y) and Characteristic Energies (E^*) of HP BN.

Ion energy (eV)	Incidence angle (^{o})	Y_{Cond} (mm^3/C)	Y_{BN} (mm^3/C)	E^* (eV)
60	0	0.004	0.010	5
100	0	0.015	0.034	25
100	15	0.015	0.034	19
100	30	0.018	0.041	10
100	45	0.016	0.037	15
200	0	0.035	0.080	61
250	0	0.053	0.122	71

C. Initial Study of Temperature Dependence of Sputter Yields.

We have performed preliminary tests to examine possible temperature dependence of the sputter yield. The results are shown in Fig. 14. There is little variation in sputter yield up until about 400 °C, then some increase beginning at ~520 °C. Similar effects were observed for borosil ($BNSIO_2$)[49], and predicted in numerical modeling for BN[23]. Discussion of possible mechanisms of thermally enhanced sputtering can be found in Ref. 24 and 50.

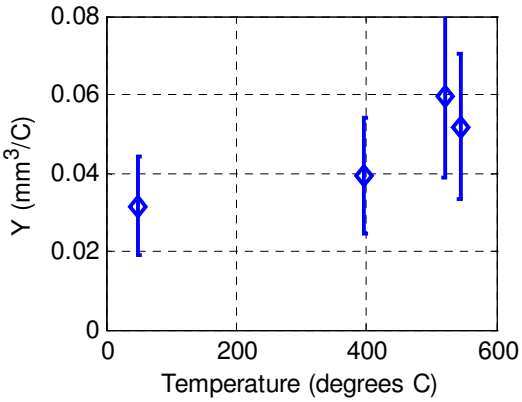

Figure 14. Thermal dependence of sputter yield for HBC-grade BN.

D. Functional Fitting of Sputter Yields.

Total sputter yield values (parameter Y in the modified Zhang expression) were fitted using a product of the Bohdansky equation[45], used to fit the energy dependence of the sputter yields, and a semi-empirical equation from Yamamura representing the angular dependence[43]:

$$Y = Y_E Y_\beta \tag{4}$$

The Bohdansky and Yamamura equations were used because they adequately describe the physical trends of the sputter yield energy and angular dependences. More general fitting functions (for example, polynomial) could possibly provide better fits to the experimental data (i.e. lower discrepancy between the experimental points and the fitting function), but they may provide very inadequate descriptions outside of the domain where experimental data are available (energy range - 60-500 eV, ion incidence angle – 0-45 degrees).

An equation developed by Bohdansky[45] is used to fit energy dependence:

$$Y_E = k\left[1-\left(\frac{E_{th}^E}{E}\right)^{2/3}\right]\left[1-\frac{E_{th}^E}{E}\right]^2 \tag{5}$$

Bohdansky altered the original Sigmund expression[34] to better match low energy sputter yields The values of k and E_{th}^E from a least squares fit of HBC data are 0.053 mm^3/C and 24±6 eV, respectively, and the resulting fit is presented in Fig. 15. Note that the normal incidence fits of Fig.15 use Eq. (4) and the full measured data set over all incidence angles, not just the normal incidence data. An expression from Zhang[40] for the energy dependence of the total sputter yield was also fitted to the experimental data, but the fit does not represent the experimental data as well

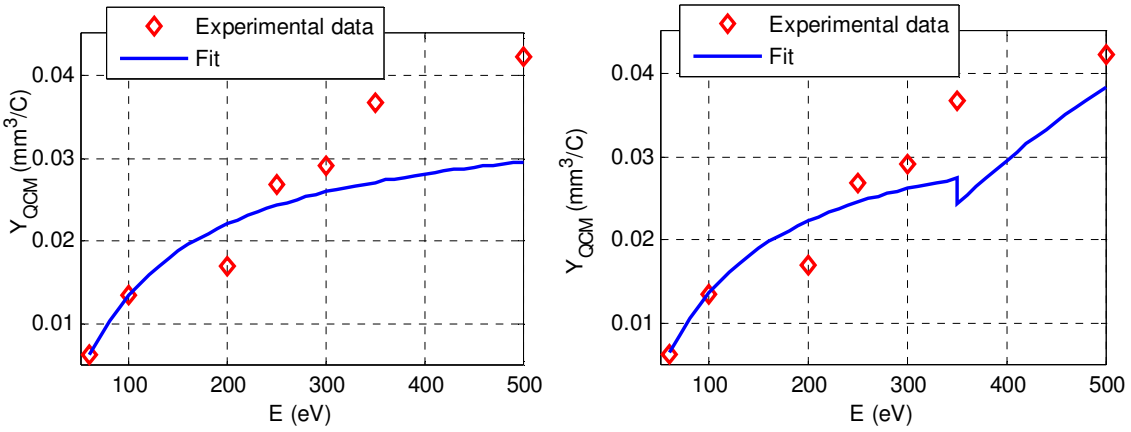

(a) **(b)**

Figure 15. HBC sputter yield at normal incidence versus ion energy (a) single fit (b) composite fit for two energy ranges.

as that from Bohdansky, especially at low energies. The threshold energy obtained from the Zhang fit was 57 eV. The lowest ion energy for which we have detected BN sputtering is 40 eV, however the experimental uncertainty was significant and the data are not reported here. At lower energies, the signal falls below our noise limit (due to both the low sputter yield and the reduced beam current), but sputtering likely continues to occur (as the value of $E_{th}^{E} = 24 \pm 6$ eV in the Bohdansky fit indicates).

For the dependence on incidence angle, a semi-empirical equation from Yamamura[43] is fitted to the HBC data:

$$Y_{\beta} = (\cos\theta)^{f} \exp\left[-\Sigma\left(\frac{1}{\cos\theta} - 1\right)\right] \tag{6a}$$

where

$$f = 1.71\left(1 + 2.5\frac{\sqrt{E_{th}^{\beta}/E}}{1-\sqrt{E_{th}^{\beta}/E}}\right) \tag{6b}$$

$$\Sigma = f * \cos\left(90 - 286\left[\frac{0.09145}{\sqrt{E}}\right]^{0.45}\right) \tag{6c}$$

As an example, the resulting fit for ion energy of 100 eV is presented in Fig. 16. The Yamamura equation uses a single fit parameter E_{th}^{β}, which we have allowed to vary independently of E_{th}^{E} (and which we constrained to be non-negative), i.e. Eq. (4), therefore uses three fit parameters, k, E_{th}^{β}, and E_{th}^{β}, the best fit values of which are shown in Table 4. Maximum error values and their standard deviations are also given for reference.

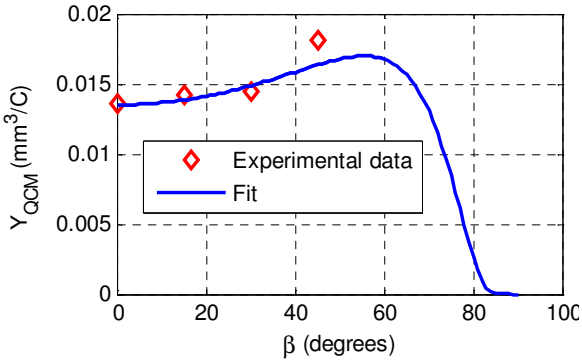

Figure 16. HBC sputter yield vs. incidence angle, 100 eV

HBC data has the highest maximum discrepancy between the experimental data and the fit. The reason is that since more data are available for HBC at lower energies, the fit reproduces these low energy values better than those at the top of the range. In an attempt to reduce the discrepancy, the fit was also applied in a piecewise way with two energy ranges: 60-300 eV and 350-500 eV. It provides a composite fit with lower discrepancy between the fitted and the experimental values, but introduces discontinuity to the fitting function. Wither low- or high-energy fit can be chosen for the range of 300-350 eV. The plots of *Y(E)* dependence including the experimental data, single fit and composite fit are shown in Fig. 15.

Table 4.

	k	E_{th}^{E}	E_{th}^{β}	Max. error,%	Error st. dev., %
HBC	0.037	24	0	40	12
HBR	0.055	29	17	34	11
HP	0.073	35	0	25	9

Table 5. Composite fit for two energy ranges (HBC).

	k	E_{th}^{E}	E_{th}^{β}	Max. error,%	Error st. dev., %

60-300 eV	0.038	23	0	29	9
350-500 eV	0.104	116	0	26	8

To capture differential sputter yield we also fit E^* values using the second-order polynomial fit:

$$E^* = c_1 E + c_2 \beta + c_3 E\beta + c_4 E^2 + c_5 \beta^2 + c_6 \tag{7}$$

The fitting parameters are given in Table 6.

Table 6.

	c_1	c_2	c_3	c_4	c_5	c_6
HBC	0.073	-0.53	0.0065	0.00037	0.0020	0.92
HBR	-0.011	0.78	0.0034	0.00079	-0.014	-0.18
HP	-0.011	0.78	0.0034	0.00079	-0.014	-0.18

Example of hemispheric differential sputter yield plots obtained using the experimental and fitted values of Y and E^* are shown in Fig. 17 and 18.

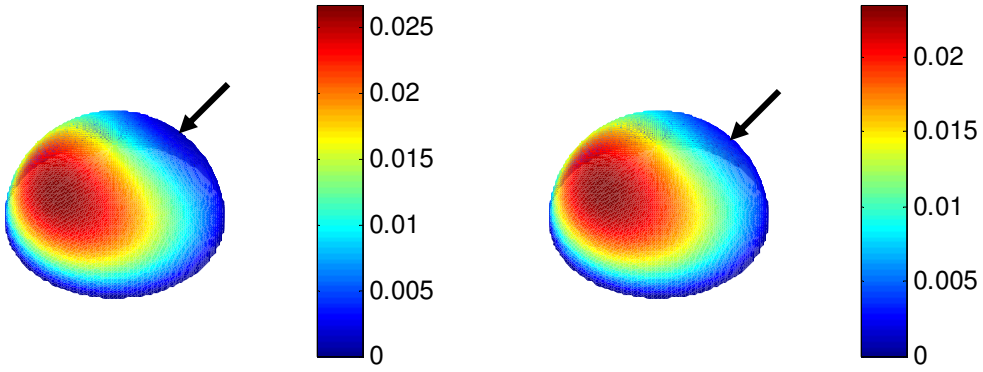

(a) **(b)**

Figure 17. Hemispherical plots of differential sputter yield for HBR, ion energy - 350 eV, incidence angle 45, (a) – using the experimental values of Y, E*, (b) using fitted values of Y, E*. Units are mm^3/C/sr.

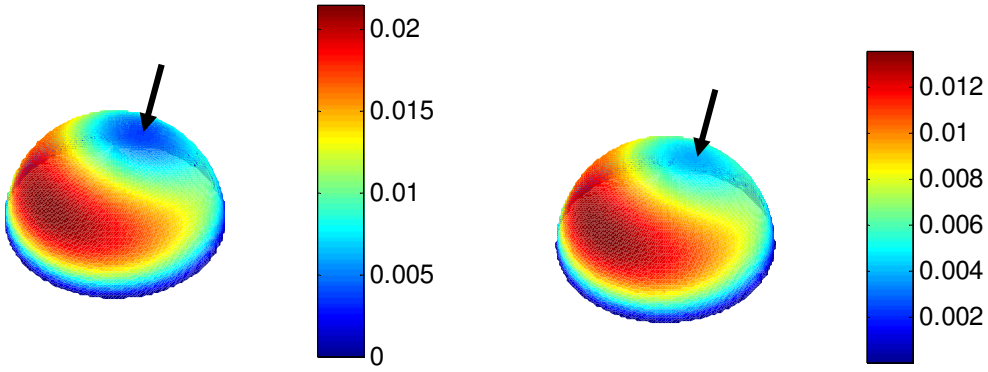

(a) **(b)**

Figure 18. Hemispherical plots of differential sputter yield for HBR, ion energy - 500 eV, incidence angle 15, (a) – using the experimental values of Y, E*, (b) using fitted values of Y, E*. Units are mm^3/C/sr.

V. Conclusion

We report total and differential sputter yield measurements for three grades of BN (HBC, HBR, and HP) in the energy range of 60-500 eV. Measurements have been performed using a QCM deposition sensor providing differential sputter yield profiles of condensable particles. Total yields are found from the integrated profiles. Using a four-grid source we have performed measurements of BN sputtering below 100 eV.

The numerical models, previously published experimental data, and our study of the QCM surface layer composition indicate that sputtering is predominantly as atoms (with boron atoms depositing to the QCM, but not nitrogen). This information is critical for interpretation of our QCM measurements and is also important for interpretation of future laser diagnostics systems based on CRDS which will measure only boron contributions. In terms of total BN sputter yields, we observe higher values relative to published data. Possible reasons for this are discussed and are under ongoing investigation. In comparison to a representative refractory metal such as molybdenum, we find similar volumetric yields for BN, though the corresponding BN mass- (or atomic-) based yields are still ~5x lower due to the lower density of BN. For HBC grade BN, the threshold energy determined by fitting experimental data is 24±6 eV. Preliminary data on the temperature dependence of the sputter yield are reported for temperature up to 544^{o}C.

Finally, we find that the fitted MZ profiles provide a reasonable description of the measured yields. The shapes (E^*/E values) for the three grades of BN are all relatively similar and show azimuthally symmetric behavior at normal incidence and forward/backward sputtering features at oblique incidence.

There is a critical need in the EP community for low ion energy sputter measurements of BN, and the present contribution is a step forward filling this gap. Upcoming and ongoing work aims to measure the BN sputtering over a broader range of sputtering conditions and includes study of variation of BN sputter yields with temperature.

Acknowledgments

The authors would like to thank Air Force Research Labs (Edwards Air Force Base, CA) for funding support. The authors also thank George Diehl and Caleb Blissett (Sigma Instruments) for help with the QCM measurement system, Paul Wilbur, John Williams and Casey Farnell (Colorado State University) for initial development of the QCM apparatus, and Cody Farnell (Colorado State University) for designing the four-grid ion optics.

References

[1]Betz, G. and Wien, K. "Energy and Angular Distributions of Sputtered Particles," *International Journal of Mass Spectrometry and Ion Processes,* Vol. 140, 1994, pp. 1-110.

[2]Tartz, M., Neumann, H., Fritsche, B., Leiter, H., and Esch, J., "Investigation of Sputter Behaviour of Ion Thruster Grid Mmaterials," *40th AIAA Joint Propulsion Conference (Ft. Lauderdale, FL),* 2004, AIAA paper 2004-4114

[3]Kolasinski, R. D., "Oblique Angle Sputtering Yield Measurements for Ion Thruster Grid Materials," *41st AIAA Joint Propulsion Conference (Tucson AZ),* 2005, AIAA paper 2005-3526.

[4]Kolasinksi, R. D., Polk J. E., Goebel D., and Johnson, L. J., "Carbon Sputtering Yield Measurements at Grazing Incidence," *42nd AIAA Joint Propulsion Conference (Sacramento, CA),* 2006, AIAA paper 2006-4337.

[5]Zoerb, K. A., Williams, J. D., Williams, D. D., and Yalin, A. P., "Differential Sputtering Yields of Refractory Metals by Xenon, Krypton, and Argon Ion Bombardment at Normal and Oblique Incidences," *29th International Electric Propulsion Conference (Princeton, NJ),* 2005, IEPC-2005-293.

[6]Yalin, A. P., Williams, J. D., Surla, V., Wolf, J., and Zoerb, K. A., "Azimuthal Differential Sputter Yields of Molybdenum by Low Energy Ion Bombardment," *42nd AIAA Joint Propulsion Conference (Sacramento, CA),* 2006, AIAA paper 2006-4335.

[7]Yalin, A. P., Williams, J. D., Surla, V., and Zoerb, K. A., "Differential Sputter Yield Profiles of Molybdenum due to Bombardment by Low Energy Xenon Ions at Normal and Oblique Incidence," *Journal of Physics D - Applied Physics,* Vol. 40**,** 2007, pp.3194-3202.

[8]Polk, J. E., "An Overview of the Results from an 8200 Hour Wear Test of the NSTAR Ion Thruster," *35th AIAA Joint Propulsion Conference (Los Angeles, CA),* 1999, AIAA paper 99-2446.

[9]Yalin, A. P., Rubin, B., Domingue, S. R., Glueckert, Z., and Williams, J. D., "Differential Sputter Yields of Boron Nitride, Quartz, and Kapton Due to Low Energy Xe^+ Bombardment," *43rd AIAA Joint Propulsion Conference (Cincinnati, OH),* 2007m AIAA paper 2007-5314.

[10]Rubin, B., Topper, J. L., and Yalin, A. P., "Total and Differential Sputter Yields of Boron Nitride Measured by Quartz Crystal Microbalance and Weight Loss", *30th International Electric Propulsion Conference (Florence, Italy),* 2007, IEPC-2007-074.

[11]Topper, J. L., Rubin, B., Farnell, C. C., and Yalin, A. P., "Preliminary Results of Low Energy Sputter Yields of Boron Nitride due to Xenon Ion Bombardment," *44th AIAA Joint Propulsion Conference (Hartford, CT),* 2008, AIAA paper 2008-5092.

[12]Yalin, A. P., Surla, V., Farnell, C., Butweiller, M., and Williams, J. D., "Sputtering Studies of Multi-Component Materials by Weight Loss and Cavity Ring-Down Spectroscopy," *42nd AIAA Joint Propulsion Conference (Sacramento, CA),* 2006. AIAA paper 2006-4338.

[13]Chiplonkar, V. T. and Rane, S. R., "Dependence of Angular Distribution of Sputtering by Positive Ions from Metal Targets on the Impact Angle," *Indian Journal of Pure and Applied Physics,* Vol. 3, 1965, p**.** 161.
[14]Tsuge, H. and Esho, S. "Angular Distribution of Sputtered Atoms from Polycrystalline Metal Targets," *Journal of Applied Physics,* Vol. 52, 1981, pp. 4391-95.
[15]Wucher, A. and Reuter, W., "Angular Distribution of Sputtered Particles from Metals and Alloys," *Journal of Vacuum Science and Technology A*, Vol. 6, 1988, pp. 2316-18.
[16]Mannami, M., Kimura, K., and Kyoshima, A., "Angular Distribution Measurements of Sputtered Au atoms with Quartz Oscillator Microbalances," *Nuclear Instruments and Methods,* Vol. 185, 1981, pp. 533-37.
[17]Wickersham, C. E. and Zhang, Z. "Measurement of Angular Emission Trajectories for Magnetron-Sputtered Tantalum," *Journal of Electronic Materials,* Vol. 34, 2005, pp. 1474-79.
[18]Shutthanandan, V., Ray, P., Shivaparan, N., Smith, R., Thevuthasan, T., and Mantenieks, M., "On the Measurement of Low-Energy Sputtering Yield Using Rutherford Backscattering Spectrometry," *25th International Electric Propulsion Conference (Cleveland, OH),* 1997, IEPC-97-069.
[19]Mantenieks, M., Foster, J., Ray, P., Shutthanandan, S., and Thevuthasan, T., "Low Energy Xenon Ion Sputtering Yield Measurements," *27th International Electric Propulsion Conference (Pasadena, CA,)* 2001, IEPC-01-309.
[20]Kundu, S., Ghose, D., Basu, D., and Karmohapatro, S. B., "The Angular Distribution of Sputtered Silver Atoms," *Nuclear Instruments and Methods in Physics Research B,* Vol. 12, 1985, pp.352-57.
[21]Surla, V. and Yalin, A. P., "Differential Sputter Yield Measurements Using Cavity Ring-Down Spectroscopy," *Applied. Optics,* Vol. 46, 2007, pp. 4057-64.
[22]Yalin, A. P., Tao, L., Yamamoto, N., Smith, T. B., and Gallimore, A. D., "Boron Nitride Sputter Erosion Measurements by Cavity Ring-Down Spectroscopy," *30th International Electric Propulsion Conference (Florence, Italy),* 2007, IEPC-2007-075.
[23]Yim, J., "Computational Modeling of Hall Thruster Channel Wall Erosion," Ph.D. Dissertation, Univ. of Michigan, Ann Arbor, MI, 2008.
[24]Cheng, S. "Modeling of Hall Thruster Lifetime and Erosion Mechanisms," Ph.D. Dissertation, Massachusetts Inst. of Technology, Cambridge, MA, 2007.
[25]Ustarroz, J., Caro, I., Corengia, P., Garmendia, I., Marcos, J., Ahedo, E., and Gonzales del Amo, J., "Specific Laboratory Testing Equipment & Methodology for Sputtering Tests of Electric Propulsion Materials," *30th International Electric Propulsion Conference (Florence, Italy),* 2007, IEPC-2007-167.
[26]Rubin, B., Topper, J. L., and Yalin, A. P., (preprint) "QCM Based System for High-Sensitivity Differential Sputter Yield Measurements," *in submission* to *Review of Scientific Instruments.*.
[27]Farnell, C. C., Williams, J. D., Wilbur, P. J., "Numerical Simulation of Ion Thruster Optics," 28*th International Electric Propulsion Conference (Toulouse, France,)* 2003 IEPC-2003-073.
[28]Zhang, L. and Zhang, L.Z. "Anisotropic Energy Distribution of Sputtered Atoms Induced by Low energy Heavy Ion Distribution," *Radiation Effects & Defects in Solids,* Vol. 160, 2005, pp. 337-47.
[29]Nikiporetz, E., Semenov, A., Shkarban, I., and Khartova, E., "Sputtering Process of BN Based Ceramic by the Flows of Noncompensated Charge Plasma," *30th International Electric Propulsion Conference (Florence, Italy), 2007* IEPC-2007-7.
[30]Garnier, Y., Viel, V., Roussel, J.-F., and Bernard, J., "Low-Energy Xenon Ion Sputtering of Ceramics Investigated for Stationary Plasma Thrusters," *Journal of Vacuum Science and Technology A,* Vol. 17**,** 1999, pp. 3246-54.
[31]Bachmann, L' and Shin, J.J., "Measurement of the Sticking Coefficients of Silver and Gold in an Ultrahigh Vacuum," *Journal of Applied Physics,* Vol. 37, 1966, pp. 242-6.
[32]http://srdata.nist.gov/xps/
[33]Abgaryan, V. K., Mikheev, S. Yu., Prokofiev, M. V., Ryzhov, Yu. A., and Shkrban, I. I., "Mass Spectra of Particles Emitted from Ceramic Surfaces Irradiated by Plasma Flows," *Bulletin of the Russian Academy of Sciences: Physics (Izvestiya Rossiiskoi Akademii Nauk. Seriya Fizicheskaya),* Vol. 70, 2006, pp. 879-82 (in Russian).
[34]Sigmund, P. "Theory of Sputtering I: Sputtering Yield of Amorphous and Polycrystalline Targets," *Physical Review,* Vol. 184, 1969,pp. 383-416.
[35]Wehner, G. K. and Rosenberg, D., "Angular Distribution of Sputtered Material" *Journal of Applied Physics,* Vol. 31, 1960, pp.177-9.
[36]Chini, T. K., Tanemura, M., and Okuyama, F., "Angular Distribution of Sputtered Ge Atoms by Low keV Ar+ and Ne+ Ion Bombardment," *Nuclear Instruments and Methods in Physics. Research B* , Vol. 119 ,1996, pp. 387-91.
[37]Yamamura, Y. and Muraoka, K., "Over-Cosine Angular Distributions of Sputtered Atoms at Normal Incidence", *Nuclear Instruments and Methods in Physics Research B,* Vol. 42**,** 1989, pp. 175-81.
[38]Yamamura, Y., "Contribution of Anisotropic Velocity Distribution of Recoil Atoms to Sputtering Yields and Angular Distributions of Sputtered Atoms," *Radiation Effects,* Vol. 55**,** 1981, pp. 49–55 .
[39]Yamamura, Y., "Theory of Sputtering and Comparison to Experimental Data," *Nuclear Instruments and Methods,"* Vol. 194**,** 1982, 515–22 .
[40]Zhang, Z. L. and Zhang, L. "Anisotropic Angular Distributions of Sputtered Atoms," *Radiation Effects & Defects in Solids,* Vol. 159**,** 2004, pp. 301-7.
[41]Zhang, J., Bhattachargee, S., Shutthanandan, V., and Ray, P. K. "Sputtering Investigation of Boron Nitride with Secondary Ion and Secondary Neutral Mass Spectrometry," *Journal of Vacuum Science and Technology A*, Vol. 15, 1997, pp. 243-7.
[42]Yamamura, Y. and Tawara, H. "Energy Dependence of Ion-Induced Sputtering Yields from Monatomic Solids at Normal Incidence," *Atomic Data Nuclear Data Tables,* Vol. 62, 1996, pp.149-253.

[43]Yamamura, Y., Itikawa, Y., and Itoh, N. "Angular Dependence of Sputtering Yields of Monatomic Solids" *Institute for Plasma Physics Report,* IPPJ AM-26, 1983.
[44]Doerner, R. P., Whyte, D. G., and Goebel, D. M., "Sputtering Yield Measurements During Low Energy Xenon Plasma Bombardment," *Journal of Applied Physics,* Vol. 93**,** 2003, pp. 5816-23.
[45]Bohdansky, J. A., "Universal Relation for the Sputtering Yield of Monatomic Solids at Normal Ion Incidence*," Nuclear Instruments and Methods in Physics. Research. B,* Vol. 2, 1984, pp. 587–91.
[46]Semenov, A. and Shkarban, I., "Ion Beam Sputtering of the Surfaces of Ion and Plasma Sources," *Rocket and Space Engineering: Rocket Engines and Power Plants,* No.3, 1991, pp. 42-53 (in Russian).
[47]Abashkin, V., Gorshkov, O., Lovtsov, A., and Shagaida, A., "Analysis of Ceramic Erosion Characteristic in Hall-Effect Thruster with Higher Specific Impulse," *30th International Electric Propulsion Conference (Florence, Italy),* 2007, IEPC-2007-133.
[48]Kim, V., Kozlov, V., Semenov, A., and Shkarban, I., "Investigation of the Boron Nitride Based Ceramics Sputtering Yield Under it's Bombardment by Xe and Kr Ions," *27th International Electric Propulsion Conference (Pasadena, CA),* 2001, IEPC-2001-073.
[49]Khartov, S.A., Nadiradze, A.B., Shkarban,I.I., Zikeeva, Y.V., "SPT's High Lifetime – Some Problems of Solution," *29th International Electric Propulsion Conference (Princeton University),* 2005, IEPC-2005-62.
[50]Doerner, R.P., Krasheninnikov, S.I., Schmid, K., "Particle-Induced Erosion of Materials at Elevated Temperature", *Journal of Applied Physics*, Vol. 91, 2004, pp. 4471-4475.